 CMES, vol.85, no.2, pp.177-192, 2012

Fluid Structure Interaction for Bird Impact Problem: Experimental and Numerical Investigation

Souli, M.[1] **and Gabrys, J.**[2]

Abstract: Bird impacts on aircraft are very common and cause significant safety threats to commercial and military aircraft. According to FAA (Federal American Aviation) regulations, aircraft should be able to land safely following specified types of bird impact on components such as radomes, windshields, engines leading edge structures and other exposed components. Thus exposed components are required to be certified for bird impact. In order to evaluate whether the aircraft is compliant to FAA requirements, several experimental tests and numerical simulations of bird impact on components need to be preformed. This paper presents an experimental and numerical investigation of bird impact on radome, a structural waterproof component that protects the radar system in aircraft and also nearby personnel from being accidentally struck by rotating antennas. In aircraft, randome structure is one of the most exposed component for bird impact. In this paper, numerical simulation of bird impact on radome component is considered, using new development of multi-material formulation and fluid structure interaction developed in LSDYNA. In order to validate the numerical results, experimental tests of bird impact on radome structural component were performed at Boeing researsh center.

Keywords: ALE, Fluid Structure Interaction, bird strike

1 Introduction

Simulation of bird impact problems and more general Fluid Structure Interaction (FSI) problems becomes more and more the focus of computational engineering in the last years. It is well known in aerospace industry that experimental tests of bird impact are expensive and time consuming. Several impact tests have been conducted by Wilbeck (1977) to describe constitutive material law of various materials including gelatine and bird. Through these studies it has been concluded

[1] Université de Lille1, Laboratoire de Mécanique de Lille, UMR CNRS 8107
[2] The Boeing Company, Boeing Co, Rotorcraft Div, Philadelphia, PA USA

at velocity above 100m/s, these materials were seen to behave as a fluid upon impact. The impact process was first dominated by an initial shock phase, with a pressure of the initial shock called Hugoniot pressure, and quickly released to a steady flow condition with a stagnation pressure. This model can be applicable to an impact of any material for which the shock pressure generated during the impact is much greater than the strength of the material but are less that the strength of the target material. Following theses analysis, it is reasonable to model the bird as a hydrodynamic model with an appropriate equation of state for the pressure. Thus bird impact on structural component can be treated as a fluid structure interaction problem. Several approaches have been used for the simulation of fluid structure interaction problems, including Lagrangian and ALE (Arbitrary Lagrangian Eulerian) formulations. Initially classical FEM Lagrangian formulation were used for the simulation of bird impact problems. Using the Lagrangian approach for bird modeling, the element size tends to become very small and distorted. Due to the extremely high material deformation and high mesh distortion of the bird model, this ultimately results in a very small computational time and often produces an unstable numerical solution. One of the commonly used approach for bird impact is the ALE multi-material or Eulerian formulation which has been used with success for problems involving large mesh distortion of the fluid mainly at the fluid structure interface.

The ALE multi-material formulation used in this paper, and developed with the collaboration of the first author in LSDYNA code, see Halquist (1998), has been validated for several academic and industrial applications. Once simulations are validated by experimental test results, it can be used as a design tool for the improvement of the structure involved. In this paper the ALE formulation for the simulation of fluid dynamics problems, as well as the coupling algorithm are presented. The paper is concentrated on the validation of the methodology that has been implemented in an explicit finite element code for structural dynamic to be able to simulate fluid structure interaction problems, where the fluid can be defined by an ALE or Eulerian mesh and the structure as a Lagrangian deformable mesh. From an algorithmic point of view, a fluid element can contain more than one fluid material, for bird impact problem, an element may contain one or two different materials, bird material and air material or void. During the simulation, state variables are computed and stored for each material in each element. An interface tracking algorithm based on Young's method, see Young (1982), is used to capture the interface between the two materials inside the element. This method was used successfully to model many industrial and academic applications as sloshing tank problem, Aquelet et al. (2005) and airbag inflation, Souli et al. (2011)

In this paper, we describe in section 2, the ALE formulation of the Navier Stokes

equation in a moving domain, and the advection algorithms used to solve mass, momentum and energy conservation. The detail of a new coupling method, Euler Lagrange Coupling algorithm, used at the fluid structure interface for structure loading is described in section 3. The description of the bird impact problem, including a detailed description of the equation of the state used for the bird and the material model used for the radome is conducted in section 4. In section 5, numerical results as well as experimental results are presented, which show good correlation concerning the location and the size of the hole from material failure during the impact.

2 ALE formulation and Coupling algorithm

2.1 ALE and Eulerian formulation

Fluid structure interaction problems, in which interfaces between different materials are present, are more easily modeled by using a Lagrangian mesh. However, if an analysis for complex structure geometry is required, the distortion of the Lagrangian mesh makes such a method difficult to use, and many re-meshing steps are necessary for the calculation to continue. Another method to use is an ALE or Eulerian formulation. This change from a Lagrangian to ALE or Eulerian formulation, however, introduces two problems. The first problem is the interface tracking, and the second problem is the advection phase or advection of fluid material across element boundaries.

To solve these problems, an explicit finite element method for the Lagrangian phase and a finite volume method (flux method) for the advection phase are used. We can refer to several explicit codes such as Pronto, Dyna3D and LS-DYNA; see Hallquist (1998) for a full description of the explicit finite element method. The advection phase has been developed into the LS-DYNA code, extending the range of applications that can be used with the ALE formulation. Current applications include sloshing involving free surface, and high velocity impact problems where the target is modeled as a fluid material, thus providing a more realistic representation of the impact event by capturing large deformations.

An ALE formulation contains both pure Lagrangian and pure Eulerian formulations. The pure Lagrangian description is the approach that: the mesh moves with the material, making it easy to track interfaces and to apply boundary conditions. Using an Eulerian description, the mesh remains fixed while the material passes through it. Interfaces and boundary conditions are difficult to track using this approach; however, mesh distortion is not a problem because the mesh never changes. In the ALE description, an arbitrary referential coordinate is introduced in addition to the Lagrangian and Eulerian coordinates. The material derivative with respect to

the reference coordinate can be described in equation (2.1). Thus substituting the relationship between the material time derivative and the reference configuration time derivative gives the ALE equation (2.1)

$$\frac{\partial f(X_i,t)}{\partial t} = \frac{\partial f(x_i,t)}{\partial t} + w_i \frac{\partial f(x_i,t)}{\partial x_i} \tag{1}$$

where X_i is the Lagrangian coordinate, x_i the Eulerian coordinate, w_i is the relative velocity. Let denote by v the velocity of the material and by u the velocity of the mesh. In order to simplify the equations we introduce the relative velocity $w = v - u$. Thus the governing equations for the ALE formulation are given by the following conservation equations (2.2) to (2.4):

Mass equation.

$$\frac{\partial \rho}{\partial t} = -\rho \frac{\partial v_i}{\partial x_i} - w_i \frac{\partial \rho}{\partial x_i} \tag{2}$$

(ii) *Momentum equation.*

The continuous form of the problem governing Newtonian fluid flow in a fixed domain consists of the governing equations and suitable initial and boundary conditions. The equations governing the fluid problem are the ALE description of the Navier-Stokes equations:

$$\rho \frac{\partial v_i}{\partial t} = div(\sigma_i) + \rho b_i - \rho w_i \frac{\partial v_i}{\partial x_j} \tag{3}$$

where σ is the stress tensor.

Boundary and initial conditions need to be imposed for the problem to be well posed.

(iii) *Energy equation.*

$$\rho \frac{\partial E}{\partial t} = \sigma_{ij} v_{i,j} + \rho b_i v_i - \rho w_j \frac{\partial E}{\partial x_j} \tag{4}$$

Note that the Eulerian equations commonly used in fluid mechanics by the CFD community, are derived by assuming that the velocity of the reference configuration is zero and that the relative velocity between the material and the reference configuration is therefore the material velocity. The term in the relative velocity in (2.3) and (2.4) is usually referred to as the advective term, and accounts for the transport of the material past the mesh. It is the additional term in the equations that makes solving the ALE equations much more difficult numerically than the Lagrangian equations, where the relative velocity is zero.

From a discretization point of view of (2.2) , (2.3) and (2.4), one point integration is used for efficiency and to eliminate locking,. The zero energy modes are controlled with an hourglass viscosity, see Benson (1992) . A shock viscosity, with linear and quadratic terms, is used to resolve the shock wave, Richtmyer et al. (1967); a pressure term is added to the pressure in the energy equation (2.4). The resolution is advanced in time with the central difference method, which provides a second order accuracy in time using an explicit method. For each node, the velocity is updated as follows:

$$u^{n+1/2} = u^{n-1/2} + \Delta t.a \tag{5}$$

where a is the nodal acceleration:

$$a = (F_{ext} + F_{int})/M$$

M is the nodal mass, and F_{ext}, F_{int} are the external end internal nodal forces.

The multi-material formulation is attractive for solving a broad range of non-linear problems in fluid and solid mechanics, because it allows arbitrary large deformations and enables free surfaces to evolve.

In the second phase, the transport of mass, momentum and internal energy across the element boundaries is computed. This phase may be considered as a 're-mapping' phase. The displaced mesh from the Lagrangian phase is remapped into the initial mesh for an Eulerian formulation, or an arbitrary undistorted mesh for an ALE formulation.

In this advection phase, we solve a hyperbolic problem, or a transport problem, where the variables are density, momentum and internal energy per unit volume. Details of the numerical method used to solve the equations are described in detail in Souli et al. (2011), where the Donor Cell algorithm, a first order advection method and the Van Leer algorithm, a second order advection method, are used. As an example, the equation for mass conservation is:

$$\frac{\partial \rho}{\partial t} + \nabla.(\rho u) = 0 \tag{6}$$

It is not the goal of this paper to describe the different algorithms used to solve equation (3.1); these algorithms have been described in detail in Aquelet et al.. (2005) and Benson (1992). Figure 1 describes the two phases for a one step explicit calculation.

2.2 Coupling Algorithm

Several coupling methods between CFD and structural dynamic solvers have been developed to solve coupling problems. Classical implicit and explicit coupling are

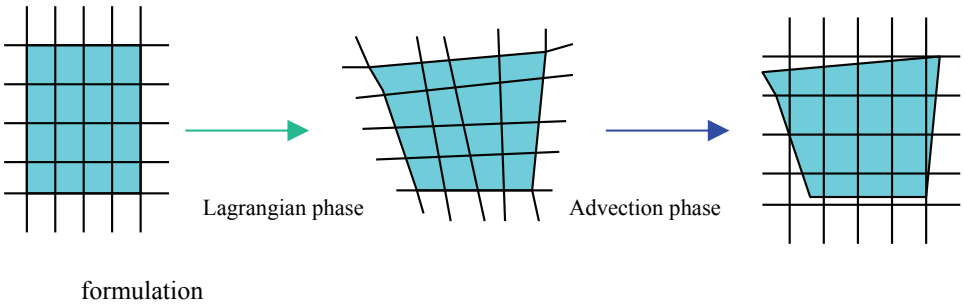

formulation

Figure 1: Lagrangian and Advection phases in multi-material ALE

described by Longatte et al. (2009), where hydrodynamic forces from the fluid solver are passed to the structure solver for stress and displacement computation. In this paper, a coupling method based on contact algorithm is used. Since the coupling method described in this chapter is based on the penalty method for contact algorithms, the contact approach is a good introduction to this method. In contact algorithms, a contact force is computed proportional to the penetration vector, which represents the amount the constraint is violated. In an explicit FEM method, contact algorithms compute interface forces due to impact of the structure on the fluid, these forces are applied to the fluid and structure nodes in contact in order to prevent a node from passing through contact interface. In contact algorithms, one surface is designated as a slave surface, and the second as a master surface. The nodes lying on both surfaces are also called slave and master nodes respectively. The penalty method imposes a resisting force to the slave node, proportional to its penetration through the master segment. This force is applied to both the slave node and the nodes of the master segment in opposite directions to satisfy equilibrium.

Penalty coupling behaves like a spring system and penalty forces are calculated proportionally to the penetration depth and spring stiffness. The head of the spring is attached to the structure or slave node and the tail of the spring is attached to the master node within a fluid element that is intercepted by the structure, as illustrated in figure 2.

Similarly to penalty contact algorithm, the coupling force is described by (3.1):

$$F = k.d \tag{7}$$

where k represents the spring stiffness, and d the penetration. The force F in figure 2 is applied to both master and slave nodes in opposite directions to satisfy force equilibrium at the interface coupling, and thus the coupling is consistent with the fluid-structure conditions, namely the action-reaction principle.

The main difficulty in the coupling problem comes from the evaluation of the stiffness coefficient k in Eq. (3.1). The stiffness value is problem dependent, a good value for the stiffness should reduce energy interface in order to satisfy total energy conservation, and prevent fluid leakage through the structure. The value of the stiffness k in (3.1) is still a research topic for explicit contact impact algorithms in structural mechanics. In this paper, the stiffness value is similar to the one used in Lagrangian explicit contact algorithms, described in Benson (1992).

The value of k is given by (3.2) in term of the bulk modulus K of the fluid element in the coupling containing the slave structure node, the volume V of the fluid element that contains the master fluid node, and the average area A of the structure element connected to the structure node.

$$k = \frac{KA^2}{V} \tag{8}$$

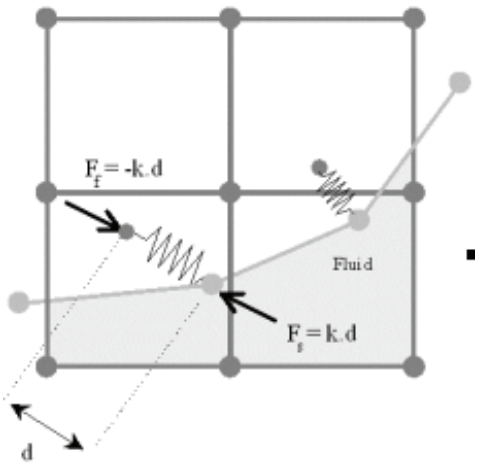

description

Figure 2: Euler Lagrange coupling

3 Description of the bird impact problem

3.1 Equation of state for the Bird material model

The first effort was to validate the material model used for the bird and the equation of state in the analysis. Several impact tests was conducted at the Air Force's

Wright Laboratory, Wilbeck (1997) for correlation purposes. The impact experiment consisted of launching materials with low strength as gelatine and bird materials on a rigid pressure instrumented plate. With the impact velocity that generates stresses on the bird material that are much higher than the strength of the material, a hydrodynamic fluid like behavior of the bird material is expected. This approximation is well established in aerospace industry for the simulation of bird impact problems. In this paper, a fluid material similar to water is used for the constitutive material law of the bird with a density slightly reduced to match the measure density of the bird. For hydrodynamic response, Mie Gruneisen equation of state is used, which defines the material's volumetric strength and pressure to density ratio. In this paper the Mie Gruneisen equation of state, implemented in LSDYNA, is used:

$$P = \rho_0 . c^2 . \frac{\mu(\mu - 1)}{(\mu - s(\mu - 1))^2} \tag{9}$$

where c is the speed of sound, $\mu = \frac{\rho}{\rho_0} - 1$, with ρ_0 and ρ the initial and current densities. The coefficient s is the linear Hugoniot slope coefficient of the shock velocity particle velosity $(U_s - U_p)$ curve,

$$U_s = c + s.U_p \tag{10}$$

U_s is the shock wave velocity and U_p the particle velocity. This equation of state requires material specific coefficient s, which is obtained through shock experiment by curve fitting of the $U_s - U_p$ relationship. Shock experiments on fluids and solids provide a relation between the shock speed U_s and the particle velocity U_p behind the shock along the locus of shocked states. For non-porous materials, and in the absence of phase transitions, these data are approximated reasonably well by a linear relation as in Wilbeck (1997).

3.2 Bird and random Constitutive material models

Bird model description

The bird was modeled as an elliptical shape made of a cylinder with hemispherical ends with a length to diameter ratio equal to 2, as illustrated in Figure 3, with major and minor dimensions selected to result in a mass of M=1.814 Kg (4 Pounds). This shape was chosen since sharp shape or regular shape such as a cylinder, could produce unrealistic impact pressure profiles. The minor radius used was 62 mm, while the major radius was 118 mm. A non viscous hydrodynamic fluid material is used for the bird with a density of 940.28 Kg/m^3.

Radome model description

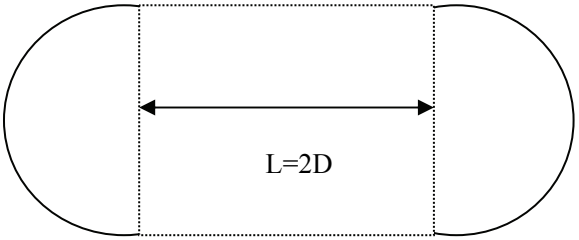

Figure 3: Geometrical shape of the bird

The radome structure is constructed from a phenolic resin-honeycomb with fiberglass face sheets. The radome is designed to withstand aerodynamic loading and be transparent to weather radar signal. The structure is lightly constrained to the fuselage by hinges, which allows for maintenance access. The radome consists of 4-ply fiberglass face sheets, with an 8 mm thick honeycomb core. This construction was modeled with a sandwich of thick shell elements. The shell face sheets were constrained to the core made of solid elements using tied contact interface.

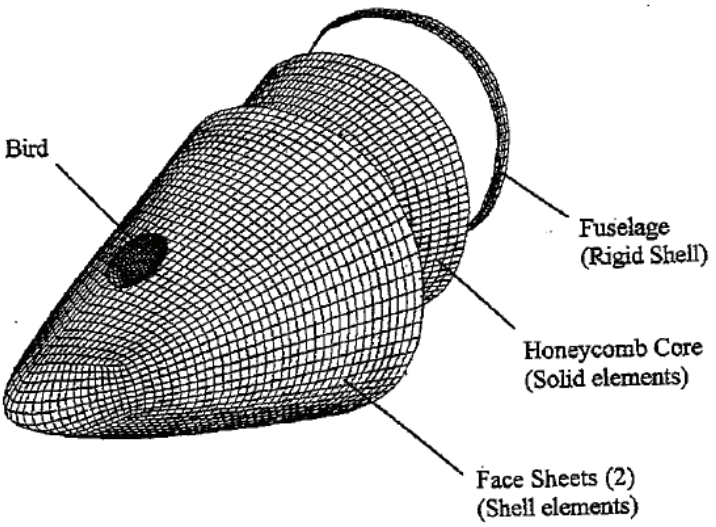

Figure 4: Detailed description of the radome

A rigid ring structure was placed at 7.6 mm behind the radome to simulate the

fuselage/radome interface, with the connecting hinges modeled as a set of linear springs. The radome was allowed to make contact with the rigid ring structure if it closed the 7.6 mm gap. The latches were modeled as springs, but were allowed only to provide a tensile load constraint. The spring constant used for the hinges were large (17.55 N/mm), so the radome would be forced to rotate about the upper hinge locations. Figure 4 shows the elements of the model in an exploded view. A schematic identifying the radome impact location is shown in figure 4. The ellipsoid "bird" was rotated about 20 degrees, to impact slightly flat on the radome. The forces created by the flatter impact would be more conservative with this approach. Some of these conditions were arbitrary, but chosen test conditions. A velocity of 174.9 m/s (340 knots) was imposed.

4 Numerical simulations

4.1 Cylindrical water impact problem

According to one dimensional Hugoniot analysis as described in Lavoie et al. (2007), bird impact with an incident velocity U_i, is characterized by two stages, the initial shock and the steady state shock called stagnation pressure. The pressure of the initial shock called Hugoniot pressure P_H is given by equation (5.1), and the steady state pressure P_S by equation (5.2).

$$P_H = \rho_{\dot{0}}.U_s.U_i \tag{11}$$

$$P_S = 1/2.\rho_{\dot{0}}.U_i^2 \tag{12}$$

To validate the Mie Gruniesen equation of state developed in LSDYNA and used in the paper, Hugoniot and static pressures are compared to the one dimensional theoretical analysis. For this purpose, we consider a cylindrical shape made of water material impacting a rigid plate at incident velocity $U_i = 100m/s$, as described in figure 5. In this analysis, the density of water $\rho = 1000kg/m^3$, the speed of sound c=1500m/s, and a Hugoniot slope parameter s in equation (4.2) is given by s=1.75. Using these data, and according to equations (5.1) and (5.2), setting the particle velocity $U_p = U_i$in these two equations, the normalized Hugoniot analytical pressure, and the normalized steady state analytical pressure are:

$$P_H/(1/2\rho.U_i^2) = 35$$

$$P_S/(1/2\rho.U_i^2) = 1.$$

In figures 6 and 7, we plot time history of the normalized pressure $P/(1/2\rho.U_i^2)$ of water impact problem described in figure 5. Normalized Hugoniot pressure given

by the initial peak pressure is shown in figure 6, and normalized steady state pressure is described in figure 7, which is a zoom of figure 6 around the normalized analytical steady state pressure equal to 1. Figure 6 shows clearly the values of the peak pressure, the Hugoniot numerical pressure:

$$P_H/(1/2\rho.U_i^2) = 34.06$$

which is in good correlation with the analytical value, within an error of 3%.

From figure 7, we observe that the normalized pressure oscillates around the value of 1 which is the normalized steady state pressure value. An estimated error of 8% is observed between analytical and numerical values.

From this example, we can see that the Mie Gruneisen equation of state with a linear $U_s - U_p$ curve, can reproduce accurately the analytical solution of the one dimensional impact problem.

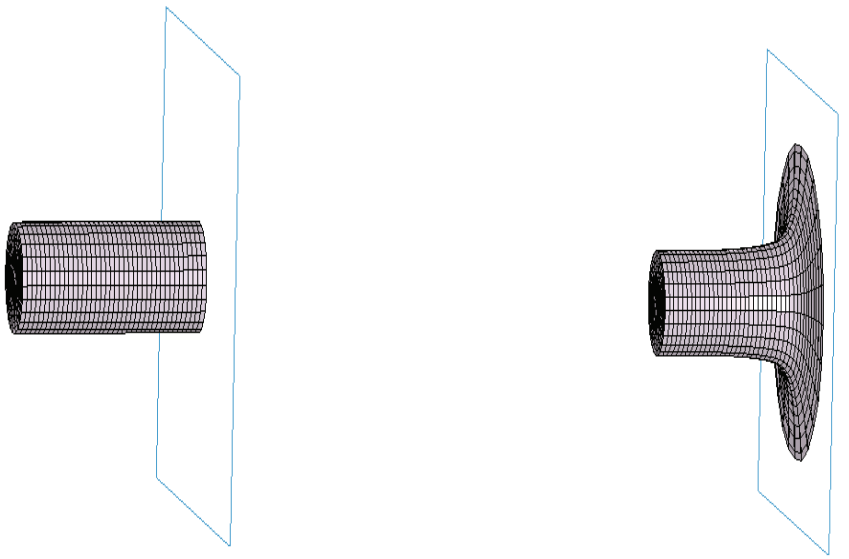

Figure 5: Water impact. mesh and deformation at t=0 , and t=3 ms

4.2 Bird impact problem

A primary assumption of the analysis is that the bird penetrates the radome by shearing a passage through the material. Therefore the shear properties of the

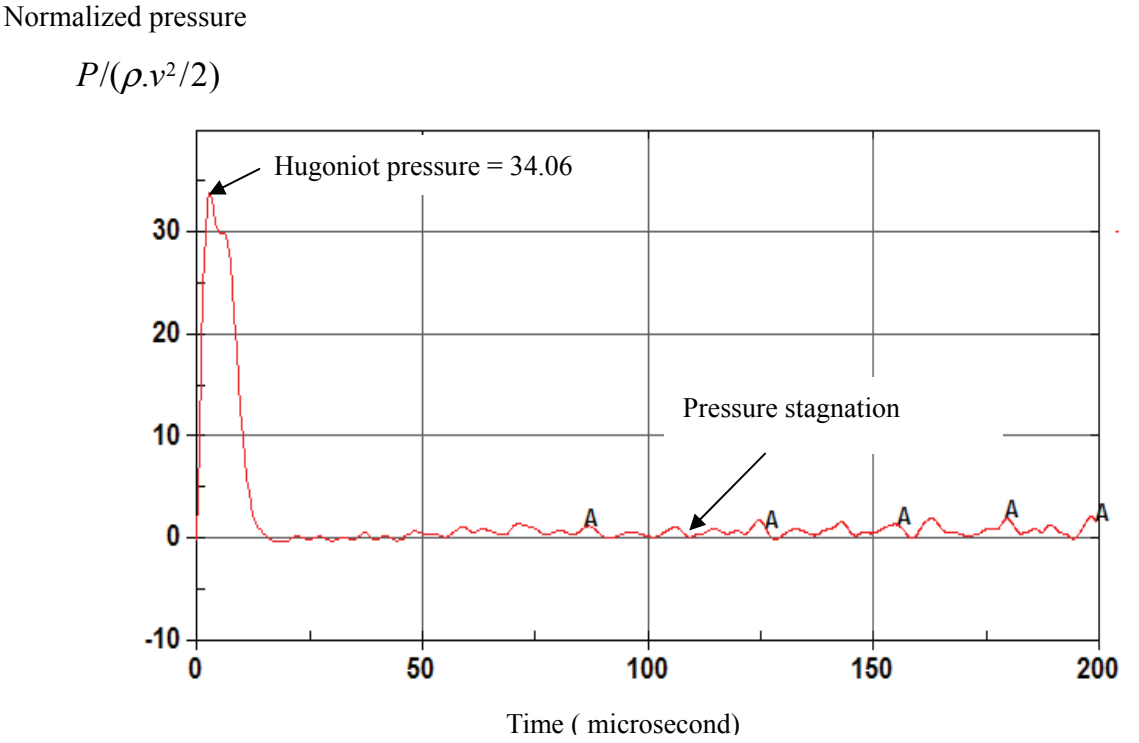

Figure 6: Pressure time history and value of Hugoniot pressure (peak pressure)

radome materials are the essential characteristics that need to be reflected in a failure criteria. The assumption is valid if the penetration velocity is significantly greater than the ballistic limit. A Von Mises yield criteria is used in the material model to predict 'yielding', and failure in the model will be assumed to occur at a specified 'plastic strain'. Therefore, a failure strain condition that results in the proper material shear allowable will be used in the material model. A yield stress that is approximately 2 times the shear allowed will produce the proper shear failure stress. For the face sheets a shear capability of 10.000 PSI was assumed, and the failure strain was assumed small ($S_y = 20.000$PSI, 0.1% plastic strain). For the epoxy-honeycomb core a shear capability of 400 PSI was assumed with some crushing of the core allowed before failure ($S_y = 500$PSI, 20% plastic strain).

Figures 8 and 9 show the simulation response of the radome from 1 to 3 milliseconds. The hole made in the radome is estimated to be about 12inch by 24inch. As seen in figure 9, some of the bird is deflected, but most continues on a path straight

Normalized pressure

$P/(\rho.v^2/2)$

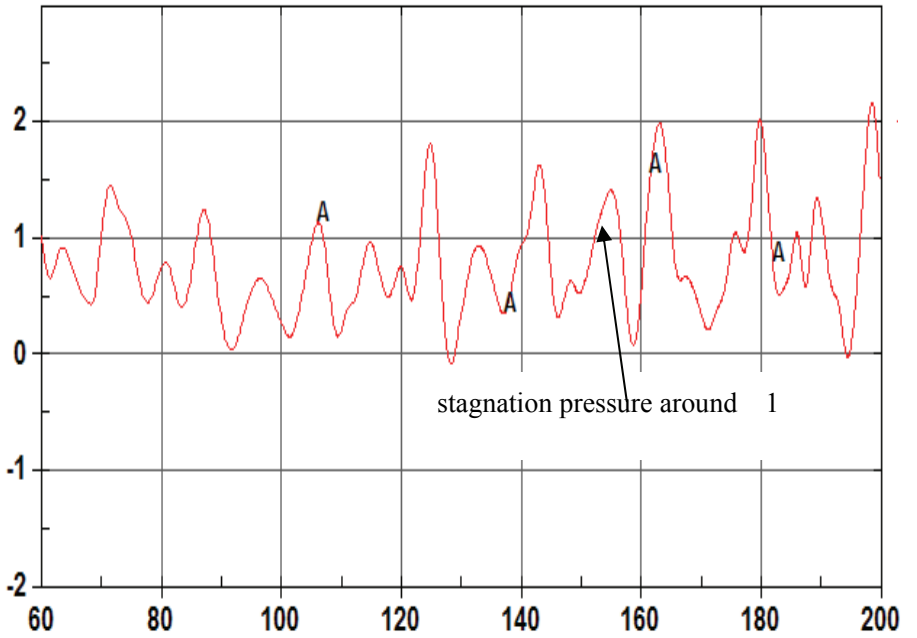

Time (microsecond)

Figure 7: Pressure time history and value of stagnation pressure

through. An estimate of the length and diameter of the residual mass of the bird appear to be about 4.5 to 5 inch long., while the width has grown to about 9 inch. A slug near aft end of the bird is nearly the starting diameter that approximate 5 inch. The simulation indicates that the bird will penetrate the radome without a significant loss of mass or velocity. It is estimated that about 10% of the mass will be deflected (0.4 pound) and the bird may be slowed about 10% . This provides some relief to downstream structure, but it is clear that the structure is not robust enough to deflect the bird. The simulation was conducted prior to any tests on the radome and was used as impetus to design a barrier behind the radome.

Testing of the radome was conducted following simulation efforts. A surrogate

forward fuselage was impacted with a 4 pounds bird lunched at 300 knots. The bird penetrated the radome, as shown in figure 10, and was stopped by a barrier structure placed forward of the main cabin pressure bulkhead. The radome hinges did not fail during the test, although a latching mechanism was latter redesigned.

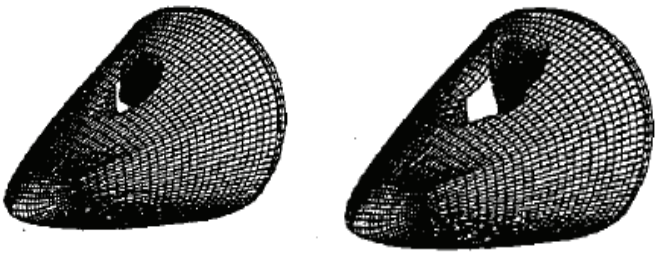

Figure 8: Simulation at time t=1.5 ms and t=2.5 ms

Since the ultimate objective is the design of a safer radome, numerical simulations can be included in shape design optimization with shape optimal design techniques, Souli et al. (1993), and material optimisation, Souli et al. (2007), Ozdemir et al. (2010). Once simulations are validated by test results, it can be used as design tool for the improvement of the system structure involved.

5 Conclusion

In this paper, a numerical simulation of bird impact on deformable structure is presented using the new LSDYNA development concerning Arbitrary Lagrangian Eulerian (ALE) approach for the bird material considered as a hydrodynamic fluid like material for this specific application. The Mie-Gruneisen equation of state using Hugoniot equation for the shock velocity particle velocity curve has been validated using a simple water impact problem on a rigid plate. For the simulation of the bird impacting a radome that protects the radar system in an aircraft, the simulation indicates that the bird would penetrate the radome without significant velocity loss or deflection. It was estimated that approximately 10% of the bird may be deflected from entering the cavity behind the radome, and the average velocity is about 10% of the initial velocity. Comparison of the test experimental results with the simulation showed very good correlation, mainly on the location and size of the

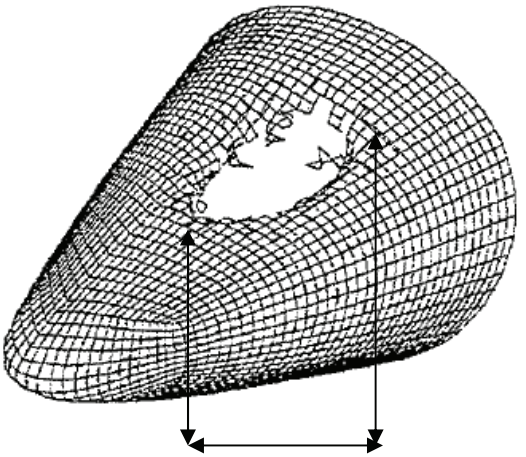

Figure 9: Simulation at time t=3 ms

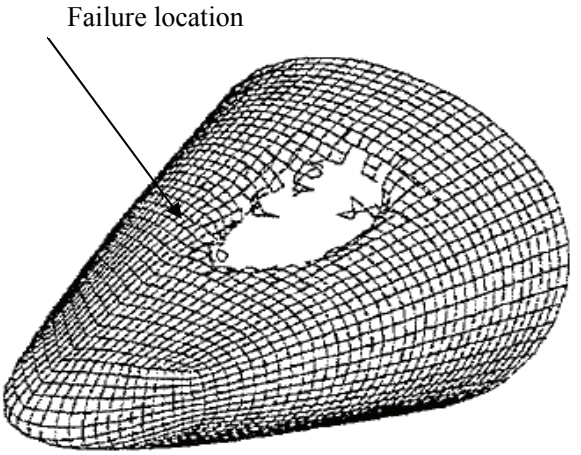

Figure 10: Numerical results of failure location at t=3 ms

hole created from failure material. The qualification of the radome and the barrier design to protect the radome was successful on the first test, avoiding any redesign effort. The simulation contributed significantly to the design of a new radome.

References

Wilbeck, J.A. (1977): *Impact behavior of low strength projectiles.*

AFML-TR pages 77-134.

Hallquist, J.O. (1998): *LS-DYNA theoretical manual*. Livermore Software Technology Company.

Young, D.L. (1982): Time-dependent multi-material flow with large fluid distortion, *Numerical Methods for Fluids Dynamics,* Ed. K. W. Morton and M.J. Baines, Academic Press, New-York.

Aquelet N., Souli M., Olovson L. (2005): Euler Lagrange coupling with damping effects: Application to slamming problems. *Computer Methods in Applied Mechanics and Engineering*, Vol. 195, pp:110-132.

Benson, D.J., (1992): Computational Methods in Lagrangian and Eulerian Hydrocodes. *Computer Methods in Applied Mech. and Eng*. Vol. 99, 235-394.

Richtmyer, R.D., Morton, K.W. (1967): *Difference Equations for Initial-Value Problems.* Interscience Publishers, New York.

Longatte E., Verreman V., Souli M. (2009): Time marching for simulation of Fluid-Structure Interaction Problems. *Journal of Fluids and Structures*, Vol. 25, No. 1, pp: 95-111.

Lavoie M.A., Gakwaya A., Nejad E., Zimcik D.G (2007): Review of existing numerical methods and validation procedure available for bird strike modeling *ICCES,* Vol.2, No.4, pp.111-118.

Souli M., Zolesio J.P. (1993): Shape Derivative of Discretized Problems. *Computer Methods in Applied Mechanics and Engineering,* Vol. 108, pp: 187–199.

Erchiqui F., Souli M., Ben Yedder R. (2007) : Nonisothermal finite-element analysis of thermoforming of polyethylene terephthalate sheet: Incomplete effect of the forming stage. *Polymer Engineering and Science*, Vol. 47, No. 12, pp: 2129-2144

Ozdemir, Z., Souli, M., Fahjan, Y. M. (2010): Application of nonlinear fluid-structure interaction methods to seismic analysis of anchored and unanchored tanks. *Engineering Structures*, Vol.32, No. 2, pp: 409-423.